Evaluation of pore size distribution via fluid-fluid displacement porosimetry: The viscous bias

Otman Maalal, Marc Prat, René Peinador, Didier Lasseux

International Journal of Multiphase Flow 149 (2022) 103983

https://doi.org/10.1016/j.ijmultiphaseflow.2022.103983

Evaluation of pore size distribution via fluid-fluid displacement porosimetry: The viscous bias

Otman Maalal [a,b], Marc Prat [a,*], René Peinador [b], Didier Lasseux [c]

[a] Institut de Mécanique des Fluides de Toulouse (IMFT), Université de Toulouse, CNRS, Toulouse, France
[b] Institut de La Filtration et des Techniques Séparatives (IFTS), Rue Marcel Pagnol, Foulayronnes 47510, France
[c] I2M, UMR 5295, CNRS, Université de Bordeaux – 351, Cours de la Libération, Talence Cedex 33405, France

ARTICLE INFO

Keywords:
Fluid-fluid displacement porosimetry
Pore size distribution
Throat size distribution
Pore network model
Numerical optimization

ABSTRACT

Fluid-fluid displacement porosimetry (FFDP) is a method for determining the pore size distribution of a porous medium from viscous fluid-fluid immiscible displacement (drainage) results, using a simplistic representation of the pore structure by cylindrical parallel tubes. The method leads to unambiguous estimates when the porous medium microstructure is strongly anisotropic and reasonably akin to this representation. The information obtained from this technique is however less straightforward to interpret for more complex microstructures. On the basis of synthetic data obtained from pore network simulations, it is evidenced, in particular, that this method leads to a shift in the distribution toward unrealistic small pore sizes. The shift, that may be very significant, is due to the viscous pressure drop in the displacing fluid. It is shown that significant improvement is achieved when the characterization of the pore size distribution is considered as an inverse optimization problem. The latter is solved using an optimization method presented in a previous work that was restricted to situations where viscous effects are unimportant.

1. Introduction

Fluid-fluid displacement porosimetry (FFDP) is a technique for characterizing the pore size distribution of a porous medium (Morison, 2008; Peinador et al., 2010; Calvo et al., 2015; Tanis-Kanbur et al., 2019). In particular, the method is commonly used for the characterization of thin porous media such as ultrafiltration and microfiltration membranes (see e.g. Peinador et al., 2010; Calvo et al., 2015; Tanis--Kanbur et al., 2019), and is traditionally referred to as the Liquid-Liquid Displacement Porosimetry (LLDP) technique since the two fluids commonly used are liquids. However, the technique can be extended to Gas-Liquid Displacement Porosimetry (Islam et al., 2020; Peinador et al., 2020) and can be simply referred to as the FFDP technique. In this method, the membrane is saturated by a wetting liquid and another immiscible liquid or gas is forced through the pores. This is accomplished through a series of pressure steps resulting in the immiscible displacement of the wetting liquid by the injected fluid (a drainage process). The injected fluid pressure at the membrane inlet is measured, as well as the injected fluid flow rate through the membrane. The dependence of these two quantities upon the pore size distribution lies in the local capillary pressure invasion threshold which must be overcome for a displacement to occur in a pore, and also in the dependency of the local flow conductances on the pore size. However, as pointed out earlier (Morison, 2008), practically all the determinations of the pore size distribution with the FFDP technique have been made considering a simplified representation of the membrane as a bundle of parallel cylindrical tubes. As analyzed in some reported works (Mourhatch et al., 2011; Maalal et al., 2021), this is quite a questionable simplification since the microstructure of most membranes significantly differs from this simplistic representation. Owing to this simplification, the question arises as to whether this technique really allows determining the pore size distribution in thin porous layers which structure departs from a simple system of cylindrical pores in parallel. The main objective of the present article is hence to clarify this question. To this end, the FFDP is simulated numerically for given microstructures. This means that the pore size distribution is perfectly known for each microstructure under consideration, without assuming cylindrical tubes in parallel. Then, the pore size distribution (PSD) is determined from the FFDP numerical simulation, i.e., from the simulated two-phase immiscible displacement in the microstructure of interest, as it would be obtained from a FFDP real experiment. The PSD estimated with this technique and the simplistic pore structure representation can finally be compared to the

real PSD in order to evaluate the possible bias and errors associated with the FFDP. According to these simulations, significant discrepancies are found between the PSD extracted from the FFDP and the real PSD. In order to improve the PSD estimation from the FFDP raw data, the PSD extraction model, based on the parallel cylindrical tubes simplification, is abandoned and a more sophisticated approach is developed. It consists in considering the PSD determination as an inverse optimization problem, which is solved using the method presented in Maalal et al. (2021). This approach is tested for various PSD, namely, uniform, Gaussian, Log-normal and bimodal. Both steps, i.e., the evaluation and assessment of the commonly used FFDP approach and the inverse optimization approach, are based on numerical simulations of the immiscible fluid-fluid displacement in the pore space of the thin porous medium under consideration. The latter are performed within the classical framework of pore network modeling (Blunt 2001, Blunt et al., 2002; Xiong et al., 2016; Bondino et al., 2013). Typically, pore network models rest on a yet simplified representation of the pore space as a system of nodes connected by narrower channels. The nodes are local larger volumes in the pore space, which, within the framework of pore network modeling, are referred to as pore bodies. The narrower channels between pores are referred to as pore throats or simply throats. In what follows, simple two-dimensional square pore networks are considered.

As illustrated in Fig. 1, the pore bodies are located at the nodes of a square regular grid and the throats correspond to the segments between nodes. The morphology of pore networks extracted from real porous media microstructures is obviously more complex than a regular grid, (see e.g. Agaesse et al., 2016; Raeini et al., 2017). However, it is expected that the crucial features for assessing the FFDP are the pore space interconnectivity (the fact that a pore body is connected to several neighboring pore bodies) and the disordered nature of the pore space (the fact that the local geometrical dimensions vary from one pore body or throat to another). These two characteristics are present in the simple pore networks considered in this study so that the main conclusions reached from this approach are expected to also apply to unstructured networks representative of the pore space of real porous media.

Within the pore network approach, the throats and pore bodies shall be considered as the two microsctructure elements to which a size distribution can be affected, namely the pore body size distribution (PBSD) and the throat size distribution (TSD), respectively. The constrictions in the pore space, which correspond to the throats, play an important role since the menisci tend to get pinned in the constrictions during a drainage process. This results from capillary effects. Moreover, the local

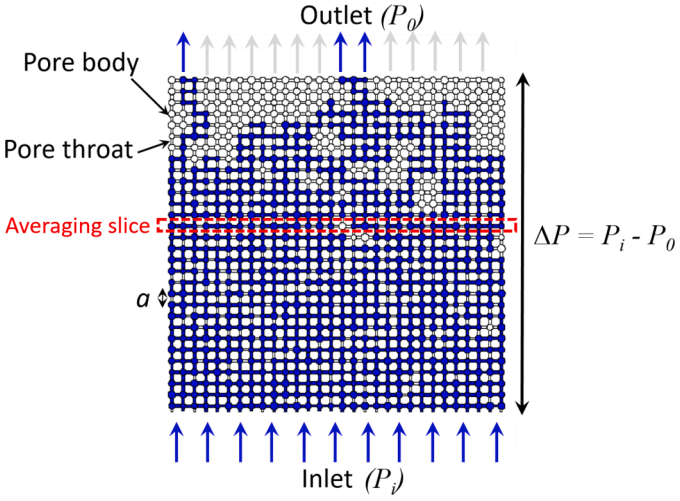

Fig. 1. Square pore network and sketch of immiscible displacement in FFDP (displacing fluid in blue, displaced fluid in light grey). The red dashed area corresponds to an exemplary network slice used for spatially averaging the pressure.

viscous pressure drops are highly dependent on the flow through the throats (the narrower the passage, the greater is the pressure drop between two pore bodies for an identical flow rate). For these reasons, the focus is laid here on the determination of the TSD.

The present study can be seen as an extension of the works presented in Mourhatch et al. (2011) and Maalal et al. (2021). In the latter reference, the immiscible displacement was simulated using the standard invasion percolation (IP) algorithm as described for instance in Wilkinson and Willemesen (1983). This corresponds to a situation where the displacement is controlled by capillary effects only. However, in a FFDP experiment, the fluid pressure is not spatially uniform in the displacing phase but decreases on average from the inlet to the outlet. For this reason, the displacement is expected to differ from that predicted by the standard IP algorithm and the flow situation corresponding to the FFDP requires a specific study. Consequently, the viscous pressure drop in the displacing fluid is taken into account, contrary to the study presented in Maalal et al. (2021). It is thus important to notice that the situation considered in the present work is much closer to operating conditions of currently available FFDP devices than the situation considered in Maalal et al. (2021). As shall be seen, the existence of the viscous pressure drop leads to an important bias in the determination of the pore size distribution if not considered in data interpretation. The identification and the illustration of this viscous bias is the major objective of the present work together with a method for alleviating its impact.

The present article is organized as follows. In Section 2, the method commonly used for determining the TSD from the FFDP raw data is recalled. The pore network model is presented in Section 3. The algorithms used to simulate the displacement and compute synthetic FFDP data is presented in Section 4. Section 5 is dedicated to the assessment of the TSD determination from the commonly used FFDP method using a parallel cylindrical tubes model. In Section 6, a method to determine the TSD from the FFDP curve using PNM simulations combined with an optimization method is briefly presented. Section 7 reports on results obtained with the optimization method when both the FFDP and retention curves are used as target data. A short discussion is presented in Section 8. Conclusions are drawn in Section 9.

2. Fluid-fluid displacement porosimetry

As indicated above and sketched in Fig. 1, the FFDP is based on the measurement of the pressure, P_i, in the displacing fluid at the inlet and the corresponding displacing fluid flow rate $Q(P_i)$. The pressure, P_o, at the outlet is fixed and considered to be the same in the displacing and displaced fluids (this point is further discussed in Section 4). The commonly used method (Morison, 2008) for determining the TSD from the flow-rate data $Q(P_i)$ in the FFDP explicitly relies on the model of a bundle of parallel cylindrical tubes. On this basis, the flow-rate is computed by applying Poiseuille's law in each tube containing the non-wetting fluid or possibly a mixed Poiseuille-Knudsen flow model in the case of GLDP (Islam et al., 2020). In what follows, Knudsen effects are not considered. Moreover, steady, laminar and incompressible flow is assumed and both fluids are supposed Newtonian. This allows writing

$$Q_i = \frac{\Delta P \pi}{8 \mu L} \int_{r_{min}}^{+\infty} r^4 f_Q(r) dr \tag{1}$$

Here, L is the tube length, $\Delta P = P_i - P_o$, μ is the displacing fluid dynamic viscosity; the radius of a tube is denoted by r and f_Q is the TSD to be determined. For a given inlet pressure P_i, the radius r_{min} is defined with the Young-Laplace equation as

$$r_{min} = \frac{2\gamma \cos\theta}{\Delta P} \tag{2}$$

where γ is the interfacial tension and θ the contact angle. In the present

work, the displaced fluid is considered as being perfectly wetting and hence, $\theta = 0$. Eq. (2) expresses that all the tubes having a radius greater or equal to r_{min} are invaded by the displacing fluid. The greater the inlet pressure, the lower is the threshold radius r_{min}. Combining Eqs. (1) and (2) leads to

$$Q_i = \frac{\pi\gamma\, cos\theta}{4\mu L r_{min}} \int_{r_{min}}^{+\infty} \rho^4 f_Q(\rho) d\rho \tag{3}$$

Considering Eq. (3) for $r_{min} = r$ and deriving the relationship with respect to r leads to

$$\frac{dQ_i}{dr} = -\frac{Q_i}{r} - \frac{\pi\gamma\, cos\theta}{4\,\mu L} r^3 f_Q(r) \tag{4}$$

and thus to

$$f_Q(r) = -\frac{4\,\mu L}{\pi\gamma\, cos\theta} r^{-3} \left(\frac{dQ_i}{dr} + \frac{Q_i}{r}\right) \tag{5}$$

Eq. (5) can be expressed in discrete form as (Morison, 2008)

$$f_{Qk}(r_{AB}) = -\frac{4\,\mu L}{\pi\gamma\, cos\theta} r_{AB}^{-3} \left(\frac{Q_{iB} - Q_{iA}}{r_B - r_A} + \frac{Q_{iAB}}{r_{AB}}\right) \tag{6}$$

where Q_{iA} and Q_{iB} are two close values of Q_i corresponding to two close values of the inlet pressure P_{iA} and P_{iB}, $Q_{iAB} = \frac{Q_{iB}+Q_{iA}}{2}$ and $r_{AB} = (r_A + r_B)/2$, r_A and r_B being determined from Eq. (2).

The value of f_{Qk} can then normalized as

$$d_{Qk}(r_{AB}) = \frac{f_{Qk}}{\sum_{i=1}^{n} f_{Qi}} \tag{7}$$

where n is the number of classes considered to compute the throat size distribution. In what follows, water is considered as the wetting fluid and air as the displacing fluid. Thus $\gamma = 0.072$ N/m and $\mu = \mu_{air} = 10^{-5}$ Pa.s.

The above equations are similar to Eqs. (9)–(14) in Maalal et al. (2021). However, there is a significant difference. In this reference, only quasi-static displacements were considered. As a result, the viscous pressure drop ΔP in Eq. (1) was assumed small compared to the capillary pressure, i.e., the pressure difference between the two fluids. As a consequence, ΔP was independent of r_{min}. The relaxation of the quasi-static hypothesis induces a modification of the radius exponent in Eqs. (5) and (6), which is now equal to -3 whereas it is equal to -4 in the corresponding equations in Maalal et al. (2021). This is because the viscous pressure drop and the capillary pressure are directly correlated as expressed by Eq. (2) in the viscous case whereas the pressure drop is independent of the capillary pressure in the QS case considered in Maalal et al. (2021).

3. Interconnected model porous medium

For FFDP, immiscible displacement is simulated in the model porous medium depicted in Fig. 1 using the pore network modeling (PNM) approach (Blunt et al., 2002). Obviously, this structure does not assume an underlying cylindrical parallel tubes structure. As illustrated in this figure, pore bodies in the pore network model are spheres of radius r_p located at the nodes of a regular square grid. The distance between two adjacent nodes is the lattice spacing a, with $a = 350$ μm in all the simulations presented below. The size of the network is the number of nodes (pores) in each direction (for example, Fig. 1 shows a 30 × 30 square network). Throats are cylindrical channels of radius r_t. The throat size is randomly distributed according to a given probability density function (p.d.f.). Similarly, the pore body sizes are distributed according to a given p.d.f. with the constraint that the size of a pore body is equal to, or greater, than the size of the largest throat to which it is connected. In the remainder of this work, the same type of p.d.f. is considered for both the pore bodies and the throats of a given network. In what follows, four types of p.d.f. are considered, namely uniform, Gaussian, Log-normal and bimodal. Also, it can be noted that the network coordination number, i.e., the number of throats connected to a pore body, is 4 in the 2D square network.

4. Fluid – fluid immiscible displacement simulation

In the FFDP, a wetting fluid is displaced by a non-wetting one, a process called drainage. It is analyzed in details by Lenormand et al. (1988), where it is shown that the resulting flow pattern depends on the competition between capillary and viscous forces. The method for computing the flow is similar to that described in this reference. Since the inlet pressure variation between two pressure steps is small, a simplification is to consider that the pressure variation in the displaced fluid between the two steady states corresponding to the two considered pressure steps can be neglected. The pressure is thus considered as uniform and equal to P_o in the displaced fluid. In fact, there is necessarily a flow in the displaced fluid and thus a viscous pressure drop during the transient period between two equilibria (equilibrium refers to the steady-state situation reached after each inlet pressure increment). However, only a small fraction of menisci moves during each transient period since the inlet pressure increments are small. As a result, the transient flow rate in the displaced fluid is small. The approximation that is performed consists in neglecting this flow and the associated displaced fluid viscous pressure drop in the identification of the moving menisci (see below). This means that the viscous flow is only computed in the sub-region of the network occupied by the displacing fluid. The displacing fluid flow computation consists in expressing the mass conservation equation at each network node (pore body) j that is given by

$$\sum Q_{i-j,k} = 0 \tag{8}$$

where $Q_{i-\,j,k}$ is the non-wetting fluid volume flow rate between pore body j and adjacent pore body k. If the throat between pore bodies j and k is occupied by the wetting fluid, then $Q_{i-\,j,k} = 0$. If the throat is occupied by the non-wetting fluid, then

$$Q_{i-\,j,k} = \frac{\pi r_{t\,j,k}^4}{8\mu_{nw} l_{j,k}} \Delta P_{j,k} \tag{9}$$

where $r_{t\,j,k}$ and $l_{j,k}$ are the radius and length of the throat connecting the two pore bodies, respectively, whereas $\Delta P_{j,k}$ is the pressure drop in the displacing fluid between the two neighboring pore bodies. The boundary conditions at the inlet and outlet of the network are $P = P_i$ and $P = P_o = const$, respectively. A zero-flux condition is imposed on the lateral faces of the network. This leads to a linear system for the pressure field at the nodes of the network in the non-wetting fluid. This system is numerically solved using the conjugate gradient method. Once the pressure field is obtained, the displacing fluid flow rate Q_i is computed using Poiseuille's law applied to all throats saturated by the displacing fluid and connected to the inlet. It can thus be noticed that the pressure is considered to be the same in the wetting fluid and non-wetting fluid at the outlet. This is an approximation. Actually, the pressure in the wetting fluid is expected to be slightly lower than in the non-wetting fluid at the outlet where the non-wetting fluid saturation remains small. The approximation consists in neglecting the pressure difference between the two fluids at the outlet compared to the viscous pressure drop, i.e. the pressure difference between the two fluids at the inlet.

The flow computation method described above applies for a given fluid distribution in the network. It must be coupled with an algorithm allowing the determination of the fluid distribution. To this end, a meniscus at the entrance of a throat is defined as stable when the pressure difference between each side of the meniscus is less than the capillary pressure threshold of the throat under consideration (such a throat is referred to as an interfacial throat), which means

$$P_{i-j,k} - P_o < P_{cth} \tag{10}$$

Here, $P_{cth} = \frac{2\gamma\cos\theta}{r_t}$ and $P_{i-j,k}$ is the pressure in the displacing fluid-saturated pore body adjacent to the throat under consideration, of radius r_t. Starting from the fluid distribution obtained at the previous step, the pressure field in the displacing fluid for the new pressure step is computed as indicated above. Then, all unstable menisci are identified. This corresponds to all menisci such that $P_{i-j,k} - P_o \geq P_{cth}$. The interfacial throat for which $(P_{i-j,k} - P_o) - P_{cth}$ is maximum is invaded with the displacing fluid together with the adjacent pore body if the latter was not already invaded in a previous step. If this pore body was occupied by the displaced fluid, new menisci are then positioned at the entrance of the throats occupied by the displaced fluid and connected to the newly invaded pore body. Thus, the list of interfacial throats is updated so as to remove the invaded throat and add the throats connected to the newly invaded pore body and occupied by the displaced fluid. This procedure is repeated until there is no unstable menisci remaining in the network, i.e., until there exists no interfacial throat for which $P_{i-j,k} - P_o \geq P_{cth}$. The resulting fluid distribution corresponds to the equilibrium distribution at the specified value of P_i.

The above procedure is enforced after the breakthrough (BT). The breakthrough corresponds to the minimum inlet pressure P_{iBT} for which the displacing fluid reaches the outlet. For inlet pressures lower than P_{iBT}, the displacing fluid does not reach the outlet and therefore there is no flow when steady state is reached. The procedure to compute the fluid distribution before BT is similar to the one described above. The important difference is that the pressure is spatially uniform and equal to P_i in the displacing fluid since there is no flow before BT when the capillary equilibrium is reached. The invasion rules described above correspond to a drainage process without trapping. An element, pore body or throat, occupied by the displacing fluid is thus assumed to be always connected to the outlet face, possibly through liquid films (Zhou et al., 1997) present in the pore and throat surface roughness and/or in a subnetwork of small crevices at the pore walls. Implementation of trapping rules is possible (see for instance Joekar-Niasar et al., 2008), but, for the sake of simplicity, trapping is not considered in what follows. In this regard, it can be recalled that trapping is exacerbated in 2D networks compared to 3D networks (Wilkinson and Willemsen, 1983). Thus, neglecting trapping can be also seen as an approximate way of considering a situation closer to the 3D case. The crucial point we keep in our approach is that menisci must travel in the pore space and that each meniscus displacement acts as a pore space local geometry probe. This point is further discussed in Section 8.

Examples of fluid distribution in a 30 × 30 2D network obtained with the procedure described above are displayed in Fig. 2 whereas the corresponding displacing fluid pressure profiles are shown in Fig. 3. The first pattern in Fig. 2 corresponds to breakthrough. The pressure plotted in Fig. 3 is the displacing fluid pressure averaged over slices containing one row of pores, successively positioned at different locations between the entrance (0) and the exit (1) of the network. Such a slice is illustrated in Fig. 1. The average displacing fluid pressure in a slice is computed as,

$$\langle P \rangle = \frac{\sum_{j=1}^{m} \frac{4\pi r_{pj}^3}{3} P_{i-j}}{\sum_{j=1}^{m} \frac{4\pi r_{pj}^3}{3}} \tag{11}$$

where m is the number of pores occupied by the displacing fluid in the

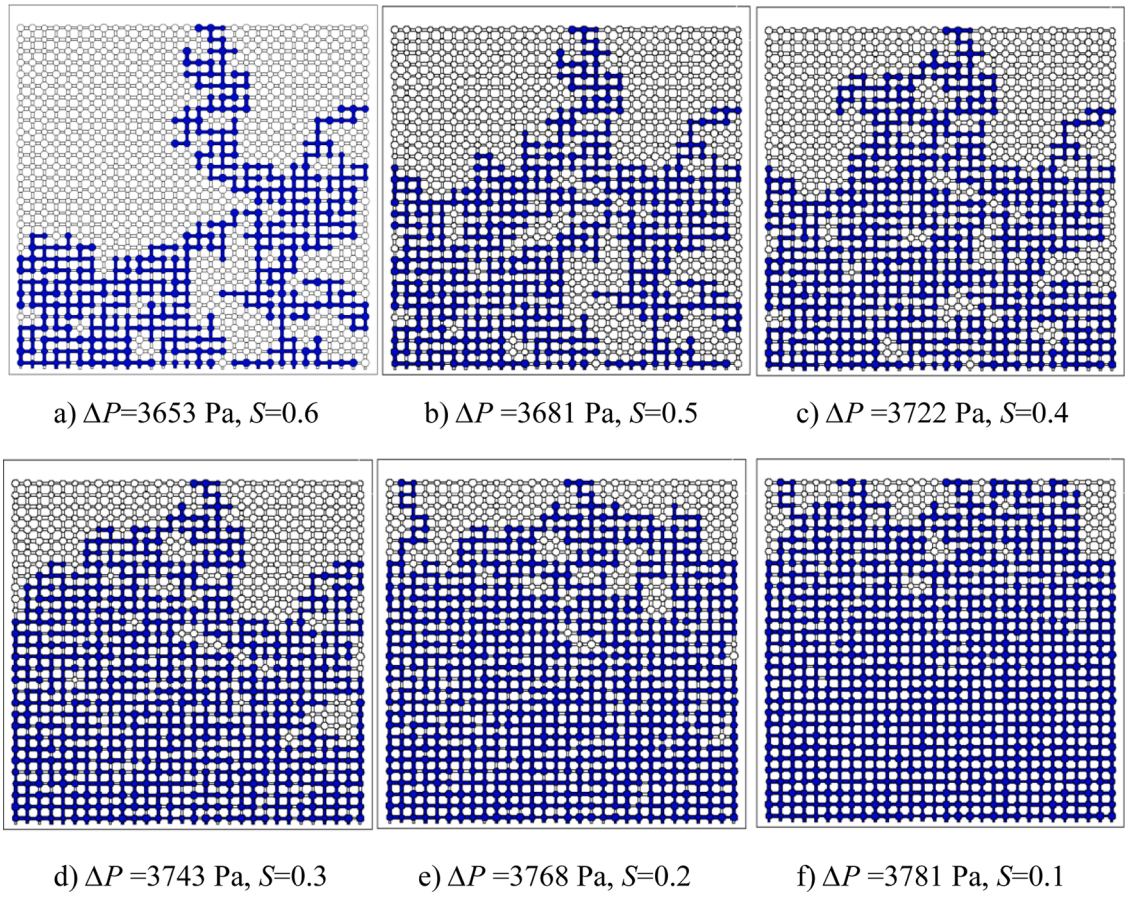

Fig. 2. Example of fluid-fluid distributions, computed in a 30 × 30 2D network with a uniform TSD (r_{tmin} = 30 μm, r_{tmax} = 50 μm) and a uniform PBSD (r_{pmin} = 80 μm, r_{pmax} = 120 μm) for an increasing pressure difference $\Delta P = P_i - P_o$. The displacing fluid in blue enters the network at the bottom. S is the displaced fluid saturation, i.e., the network volume fraction occupied by the displaced (wetting) fluid. (a) At BT. (b) to (f) After BT. (a) ΔP=3653 Pa, S=0.6 (b) ΔP =3681 Pa, S=0.5 (c) ΔP =3722 Pa, S=0.4. (d) ΔP =3743 Pa, S=0.3 (e) ΔP =3768 Pa, S=0.2 (f) ΔP =3781 Pa, S=0.1

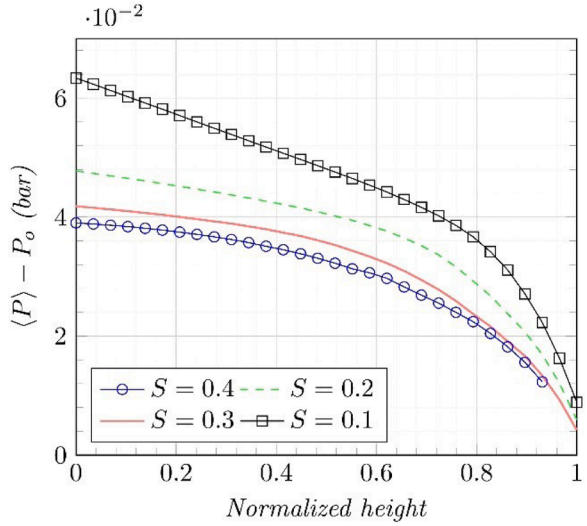

Fig. 3. Displacing fluid slice average pressure profiles in the 30 × 30 network corresponding to the fluid distributions depicted in Fig. 2. Note that the pressure is averaged over 30 realizations whereas only one realization is of course shown in Fig. 2. The inlet and outlet respectively correspond to a normalized height equal to 0 and 1.

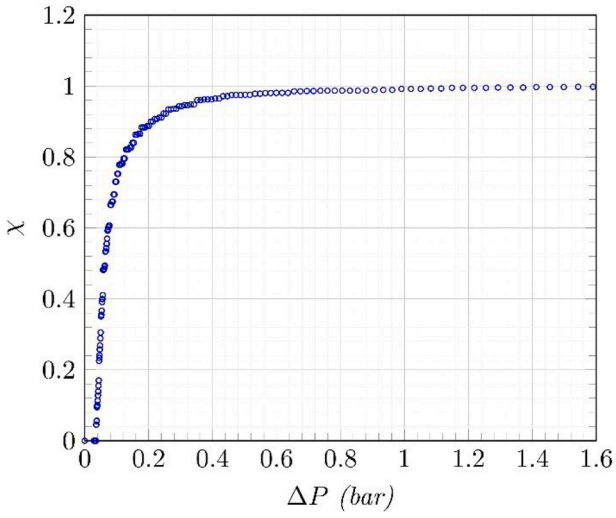

Fig. 4. FFDP curve: displacing normalized fluid flow rate, χ, as a function of $\Delta P = P_i - P_o$.

slice.

As can be seen from Fig. 2, the displacement occurs in comparatively a larger number of throats and pore bodies in the lower region of the network, that is the region adjacent to the inlet, than in the upper region of the network. This is fully consistent with the existence of the non-linear viscous pressure drop in the displacing fluid illustrated in Fig. 3. Consider two interfacial throats of the same radius. Such a throat is invaded by the displacing fluid when $P_{i-j,k} - P_o \geq P_{cth}$. The closer the throat to the inlet, the greater is the local pressure $P_{i-j,k}$ (see Fig. 3). As a result, in the sequence of pressure steps, a throat closer to the inlet is invaded before a throat of comparable radius located further away in the network. This also means that throats of different radii are invaded when the inlet pressure is incremented. For a given inlet pressure, since $P_{i-j,k}$ decreases on average with the increasing distance from the inlet, the critical invasion threshold radius given by the equation $P_{i-j,k} - P_o = P_{cth} = \frac{2\gamma cos\theta}{r_t}$ increases with the increasing distance from the inlet. In other words, results illustrated in Figs. 2 and 3 clearly indicate that there is not a unique value of the threshold pore radius given by the Young-Laplace Eq. (2) for a given value of the inlet pressure. This is in contrast with the common FFDP assumption, for which a single pore radius is associated to each inlet pressure value. This also differs from the IP approach followed by Maalal et al. (2021). In fact, the situation considered in the present article can be analyzed as a situation of invasion percolation in a stabilizing gradient (IPSG) (Xu et al., 1998). The gradient in the pore occupation probability leads to the formation of a stable invasion front corresponding, in Fig. 2, to the gradual shrinkage of the two-phase zone, which localizes here on the outlet side of the network.

The FFDP curve obtained from the algorithm above described is shown in Fig. 4. Note that this curve corresponds to one realization of the network and does not result from an average over several realizations (contrary to the pressure curves in Fig. 3). This curve typically shows the displacing fluid flow rate as a function of the pressure difference $\Delta P = P_i - P_o$. Throughout the article, the displacing fluid flow rate, Q_i, is normalized. More precisely, the quantity $\frac{Q_i}{P_i - P_o}$ is considered and normalized by $\frac{Q_{if}}{P_{if} - P_o}$, Q_{if} and P_{if} being the final displacing fluid flow rate and inlet pressure, respectively. Thus, the quantity represented in Fig. 4 is

$$\chi = \frac{Q_i \left(P_{if} - P_o\right)}{Q_{if}(P_i - P_o)} \tag{12}$$

It must be noted that χ should not be mistakenly identified as the displacing fluid relative permeability (k_r) employed in the classical theory of two-phase flow in porous media (Dullien, 1991). Indeed, χ would correspond to k_r if the fluid distributions were obtained via quasi-static displacements controlled only by the capillary effects. Owing to the viscous pressure drop in the displacing fluid, this is obviously not the case in the situation under study. To this extend, χ can be seen as a "dynamic" relative permeability.

5. TSD extraction from commonly used FFDP procedure

The next step is to apply the TSD extraction procedure commonly used for FFDP, i.e., Eqs. (1) to (7), starting from the computed FFDP curve (Fig. 4). The objective is to analyze how the TSD obtained with this procedure (Eq. (6)), referred to as the FFDP TSD, compares with the real TSD. A 2D square 50 × 5, a 2D square 50 × 25 and a 2D square 30 × 30 networks were considered for the comparison. Note that the second value in the network size nomenclature denotes its height in the main flow direction. For each network, the $\chi(\Delta P)$ curve was computed and the FFDP TSD extracted using Eq. (6). For a given network size and distribution, the results were averaged over 100 network realizations so as to eliminate dispersion of the results. For a given network size, the FFDP TSD was extracted from each $\chi(\Delta P)$ curve yielding 100 FFDP TSD which were finally averaged to obtain the FFDP TSD for the network under concern. The comparison was performed for two types of p.d.f., namely, uniform and Gaussian. The p.d.f. parameters are the throats and pore bodies minimum and maximum radii, r_{pmin}, r_{pmax} and r_{tmin}, r_{tmax} for a uniform distribution, the mean pore and throat radii, r_{pmoy}, r_{tmoy} and standard deviation, σ, in the case of a Gaussian p.d.f.. The p.d.f. parameters considered in this section are reported in Table 1.

The comparison between the real TSD and the FFDP TSD for the various cases is presented in Fig. 5 and Table2. As can be seen, the FFDP TSD is significantly different from the real TSD for all the cases

Table 1
PBSD and TSD parameters considered in Section 5.

p.d.f	Pore bodies	Throats
uniform	$r_{pmin} = 80$ µm, $r_{pmax} = 120$ µm	$r_{tmin} = 30$ µm, $r_{tmax} = 50$ µm
Gaussian	$r_{pmoy} = 120$ µm, $\sigma = 10$ µm	$r_{tmoy} = 40$ µm, $\sigma = 10$ µm

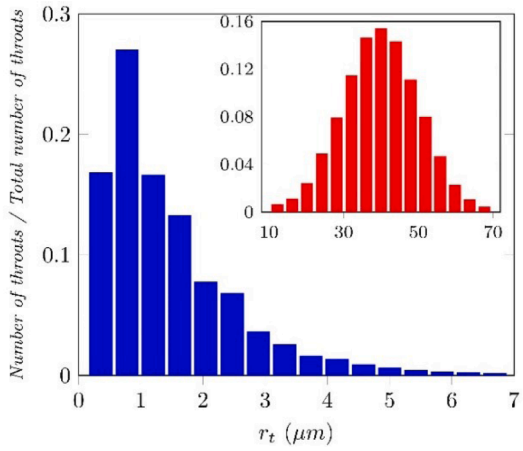

a) 50 × 5 network, Gaussian p.d.f., r_{tmoy} = 40 μm, σ = 10 μm

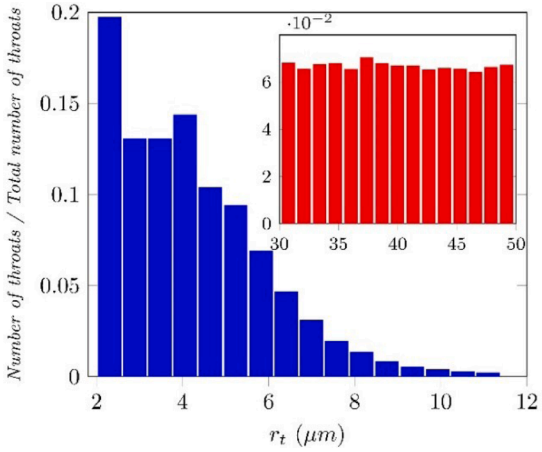

b) 50 × 5 network, uniform p.d.f., r_{tmin} = 30 μm, r_{tmax} = 50 μm

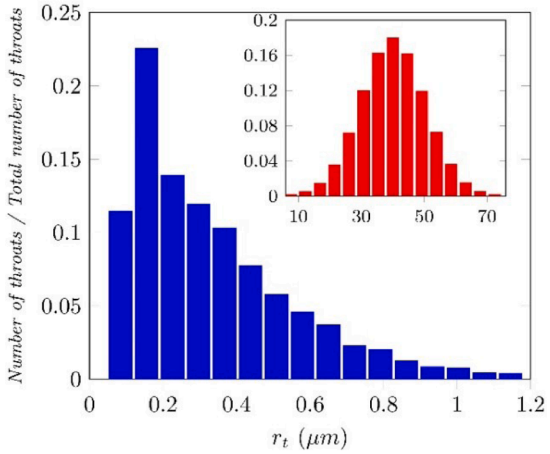

c) 50 × 25 network, Gaussian p.d.f., r_{tmoy} = 40 μm, σ = 10 μm

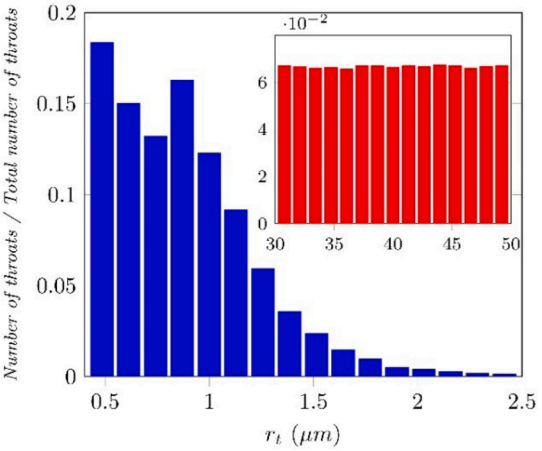

d) 50 × 25 network, uniform p.d.f., r_{tmin} = 30 μm, r_{tmax} = 50 μm

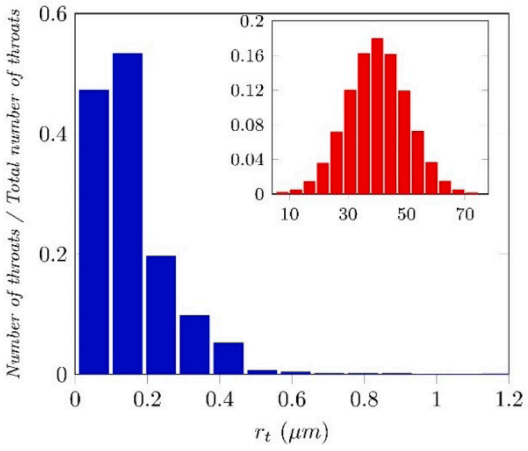

e) 30 × 30 network, Gaussian p.d.f., r_{tmoy} = 40 μm, σ = 10 μm

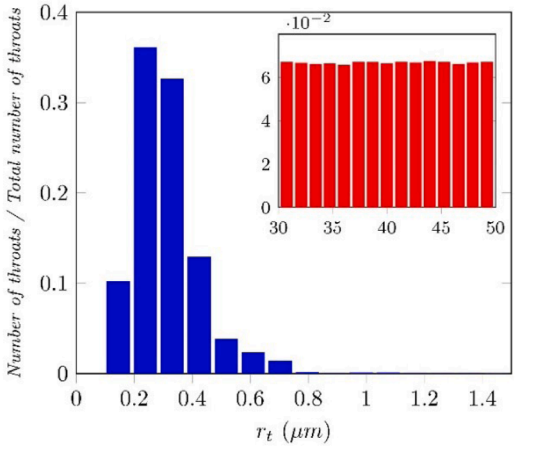

f) 30 × 30 network, uniform p.d.f., r_{tmin} = 30 μm, r_{tmax} = 50 μm

Fig. 5. Comparison of the TSD obtained from the commonly used FFDP procedure, Eq. (6), and the real TSD (shown in the insets) for various cases. **(a)** 50 × 5 network, Gaussian p.d.f., r_{tmoy} = 40 μm, σ = 10 μm. (b) 50 × 5 network, uniform p.d.f., r_{tmin} = 30 μm, r_{tmax} = 50 μm. (c) 50 × 25 network, Gaussian p.d.f., r_{tmoy} = 40 μm, σ = 10 μm. (d) 50 × 25 network, uniform p.d.f., r_{tmin} = 30 μm, r_{tmax} = 50 μm. **e** 30 × 30 network, Gaussian p.d.f., r_{tmoy} = 40 μm, σ = 10 μm. (f) 30 × 30 network, uniform p.d.f., r_{tmin} = 30 μm, r_{tmax} = 50 μm.

Table 2
Comparison between the real TSD and the TSD obtained from the commonly used FFDP procedure (Eq. (6)), i.e., the FFDP TSD. Mean values and standard deviations were computed over the 100 realizations.

	StatisticalMoments (μm)	Real TSD	FFDP TSD	RelativeError (%)
Uniform p.d.f. 50 × 5 network	Mean	39.95	4.21	89.47
	Standard deviation	5.74	1.67	70.83
Gaussian p.d.f. 50 × 5 network	Mean	39.97	1.44	96.41
	Standard deviation	10.28	1.1	89.29
Uniform p.d.f. 50 × 25 network	Mean	40.01	0.88	97.8
	Standard deviation	5.76	0.34	94.1
Gaussian p.d.f. 50 × 25 network	Mean	40.02	0.34	99.16
	Standard deviation	10.2	0.22	97.82
Uniform p.d.f. 30 × 30 network	Mean	39.99	0.31	99.23
	Standard deviation	5.75	0.12	97.89
Gaussian p.d.f. 30 × 30 network	Mean	40.01	0.15	99.62
	Standard deviation	10.29	0.12	98.86

considered here. The FFDP procedure introduces a significant positive skewness. In addition to the noticeable asymmetry, it can be seen that the FFDP procedure leads to identify throat sizes smaller than in the real TSD. This is qualitatively consistent with the experimental results reported in Peinador et al. (2020), showing a shift toward smaller pore sizes between the pore size distribution determined from the FFDP and the one deduced from the capillary pressure curve. The shift can be explained as follows. As illustrated in Fig. 2, the region near the inlet is preferentially invaded due to the greater displacing fluid pressure. When the inlet pressure is sufficiently large, menisci are only present at some distance from the inlet where the pressure in the displacing fluid is less than at the inlet. The minimum size identified from Eq. (1) is $r_{min} = \frac{2\gamma\ cos\theta}{P_i - P_0}$ whereas the actual minimum size must be determined not at the inlet where there is no menisci anymore but where menisci are present, thus $r_{min-real} \approx \frac{2\gamma\ cos\theta}{P(z) - P_0}$ where z is the distance from the inlet where the less advanced menisci, i.e. the menisci the closest to inlet, can be found. Since $P(z) - P_0 < P_i - P_0$, $r_{min}. < r_{min-real}$. Hence, the throat sizes extracted from Eq. (1) are eventually much smaller than the sizes of the throats in which the menisci are actually moving since they move in a region where the displaced fluid pressure is significantly lower than the inlet pressure. The higher the inlet pressure, the greater is the impact since, as discussed before, the two-phase zone, i.e., the zone containing the menisci, shrinks and localizes on the outlet side of the network while increasing the inlet pressure (Fig. 2). The shift is therefore due to the viscous pressure drop and the use of Eq. (1) wrongly considering the inlet pressure and not the lower pressures in the region where the menisci actually move.

As reported in Table 2, the errors associated with the parallel cylindrical tube simplification is very significant. In summary, the nature of the distribution, uniform or Gaussian, is not retrieved and the identified sizes are too small. The comparison of the FFDP TSD with the real TSD for the two networks, in Fig. 5, shows that the shift in the distribution toward unrealistic small throat sizes depends on the network height, i.e., the distance between the inlet and the outlet measured in lattice spacing unit corresponding to the number of elements (pores or throats) over the network height. The greater the height, the more pronounced is the shift. This is consistent with the above consideration on the wrong use of Eq. (1) since the greater the height the greater the inlet pressure must be to displace the menisci near the outlet. This is an indication that the commonly used FFDP TSD extraction method should not be used, in particular for the characterisation of thick porous materials.

The results presented in Fig. 5 and Table 2 are consistent with the fluid distributions and the pressure profiles depicted in Figs. 2 and 3. As discussed previously, the existence of the pressure drop across the network is not consistent with the identification of a single throat size from the Young-Laplace equation, as assumed in the commonly used FFDP procedure. In order to fully invade the network, the pressure difference between the two fluids in the outlet region of the network must be comparable to (slightly greater than) the throat capillary pressure thresholds. Since the displacing fluid pressure is significantly higher in the network inlet region, using the inlet pressure P_i together with the Young-Laplace equation leads necessarily to underestimate the throat sizes. Since the viscous pressure drop increases with the network height, greater inlet pressures are necessary to fully invade the network when its height is increased. This is consistent with the increase in the shift toward smaller throat sizes with an increasing network size reported in Fig. 5.

6. Alternative method for the FFDP TSD extraction

6.1. Method of solution

Owing to the serious shortcomings inherent to the commonly used FFDP TSD extraction procedure, the question arises as to whether a better procedure can be devised. As shown in the previous section, the standard and commonly used FFDP TSD extraction procedure does not allow determining the real TSD from the $Q_i(\Delta P)$ curve. The main reason explaining this unsatisfactory estimation lies in the fact that throats of various sizes are invaded when the pressure is incremented due to the displacing fluid pressure variation across the porous medium whereas only a single throat size is assigned via the Young-Laplace Eq. (2) to all the newly invaded throats with the commonly used FFDP procedure, regardless of their actual sizes. This notably introduces a shift toward (unrealistic) small throat sizes.

In order to improve the estimation, the TSD identification problem is addressed as an inverse problem. The direct problem is the determination of the $Q_i(\Delta P)$ curve for a given microstructure. The inverse problem consists in identifying the TSD from the $Q_i(\Delta P)$ curve and is treated with an optimization procedure in what follows. The general idea is to gradually modify the microstructure (more precisely the sizes assigned to the throats for a given network structure) so as to retrieve the $Q_i(\Delta P)$ curve accurately. To this end, the method presented in Maalal et al. (2021) is used. In this reference, the objective was to identify the TSD from the displacing fluid relative permeability and the retention curve whereas here, the objective is to identify the TSD from the FFDP curve. As in the previously mentioned work, it is assumed that the pore network structure is known. This means that the optimization procedure is performed for a given type of network, i.e., a square network in the present study. Again, the unknown is the TSD. The pore body sizes are not considered in the optimization procedure on the ground that the FFDP flow is essentially controlled by the throats. Thus, the pore size is taken as constant (equal to 80 μm) in what follows. A particular realization of the network, with specified p.d.f. parameters, is used as the reference network whose TSD is hence known. This reference network is the equivalent of the porous medium to be characterized in practice, that is, the one for which the experimental measurement of $Q_i(\Delta P)$ would have been performed in practice and whose TSD is to be determined.

The optimization procedure is actually fully identical to the one described in Maalal et al. (2021), considering χ as defined by Eq. (12) in place of Q_n in the latter reference. For this reason, the optimization algorithm is not described again here. The reader is referred to the above-mentioned article for the details. In essence, the procedure consists in gradually modifying the throat sizes in the network so as the FFDP curve of the optimized network matches the FFDP curve of the reference network using a hybrid genetic and hill climbing algorithm.

6.2. Results

A reference network, with a Gaussian TSD having a mean radius of 40 μm and a standard deviation of 10 μm, is first considered. The corresponding reference TSD is shown in the inset of Fig. 6a. Note that the initial network population in the optimization process is generated with uniform distributions, thus with a type of p.d.f. different from the Gaussian distribution of the reference network.

As shown in Fig. 6b, the optimization procedure leads to an almost perfect agreement between the $\chi(\Delta P)$ curves for the reference and optimized networks. Compared to the commonly used FFDP procedure (Fig. 5), the identified TSD is much closer to the reference TSD. There is no shift toward unrealistic small throat sizes and the distribution is much closer to a Gaussian distribution. However, one can note a slight positive skewness. The values for the first four moments of the distribution reported in Table 3 are also in much better agreement with the corresponding values of the real TSD (as can be seen from the comparison with the values reported in Table 2 obtained for the commonly used FFDP procedure).

As reported in Fig. 7 and Table 3, somewhat similar results are obtained when the reference p.d.f. is uniform. In both cases, it can be seen that a few throat sizes greater than the largest throat size in the reference distribution are obtained through the optimization procedure. This is due to the specification of the maximum throat size in the optimization procedure. As explained in Maalal et al. (2021), the maximum throat radius is approximately specified by multiplying by a factor 1.3 the radius corresponding to the first pressure step at which the displaced fluid saturation is no longer equal to one. The factor 1.3 is introduced because the biggest throat at the inlet can be expected to be smaller than the biggest throat in the whole network. Nevertheless, the fraction of throat sizes in this too large range is quite low. This is an indication that the optimization procedure should lead to still better results with a more refined estimate of the maximum throat radius (via smaller pressure steps for example).

Table 3
Comparison between the reference TSD and the optimzed TSD. Case where the reference TSD is the Gaussian TSD depicted in the inset in Fig. 6a.

	Gaussian			uniform		
		Optimized network			Optimized network	
Statistical Moments (μm)	Real TSD	Obtained TSD	Relative Error (%)	Real TSD	Obtained TSD	Relative Error (%)
Mean	42.05	43.65	3.8	41.16	42.8	3.98
Standard deviation	10.2	13.16	33.33	6.08	7.19	18.25
Skewness	-0.22	0.41	-	-0.6	-0.34	-
Kurtosis	2.71	2.95	8.86	1.81	1.71	5.44

7. TSD extraction combining FFDP and retention curves

7.1. Method of solution

It was shown in Maalal et al. (2021) that the inversion optimization procedure, considering the displacing fluid relative permeability and the retention curve, led to better results than when only the displacing fluid relative permeability was considered. Thus, one can wonder whether considering the retention curve in addition to the FFDP curve could improve the TSD identification in the case under study here. The retention curve corresponds to a series of capillary quasi-static equilibria within the porous medium and is a classical characterization of the material, also for thin porous media of special interest in the present study (see e.g. Fairweather et al., 2010). However, this implies in practice to perform an additional experiment since the FFDP devices are typically not adapted to measure the retention curve. Examples of specific measurement devices adapted to thin porous media are described for instance in Fairweather et al. (2010) and Gostick et al. (2008). To obtain the drainage retention curve, the procedure is somewhat similar to the FFDP procedure. The porous medium is initially saturated by a wetting fluid. Then a non-wetting fluid is injected through a series of pressure steps. An important difference compared to the FFDP devices is the presence of a porous membrane with smaller pores than in the medium of interest at the outlet, preventing the non-wetting fluid to exit the porous medium. Thus, contrary to the FFDP, there is no displacing fluid flow in the porous medium when an equilibrium is reached. An important difference lies also in the fluid-fluid distribution. In the case of the retention curve, the fluid-fluid distributions are quasi-static, only controlled by capillary effects. By contrast, as illustrated in Fig. 2, the fluid-fluid distributions are affected by the viscous pressure drop in the displacing fluid in the case of the FFDP. The retention curve is the graph of the pressure difference, $P_c = P_{nw} - P_w$, between the two fluids as a function of the wetting fluid saturation, S, P_{nw} and P_w being respectively the pressure in the non-wetting and wetting fluids, whereas S is the volume fraction of the pore space occupied by the wetting fluid. It should be clear that the wetting fluid (the non-wetting fluid, respectively) corresponds to the displaced fluid (the displacing fluid, respectively) in the FFDP. The couple of fluids is, however, not necessarily the same in the FFDP and the retention curve measurement since two separate measurement devices are used. In what follows, it is therefore assumed that both the FFDP curve, $\chi(\Delta P)$, and the retention curve, $P_c(S)$,

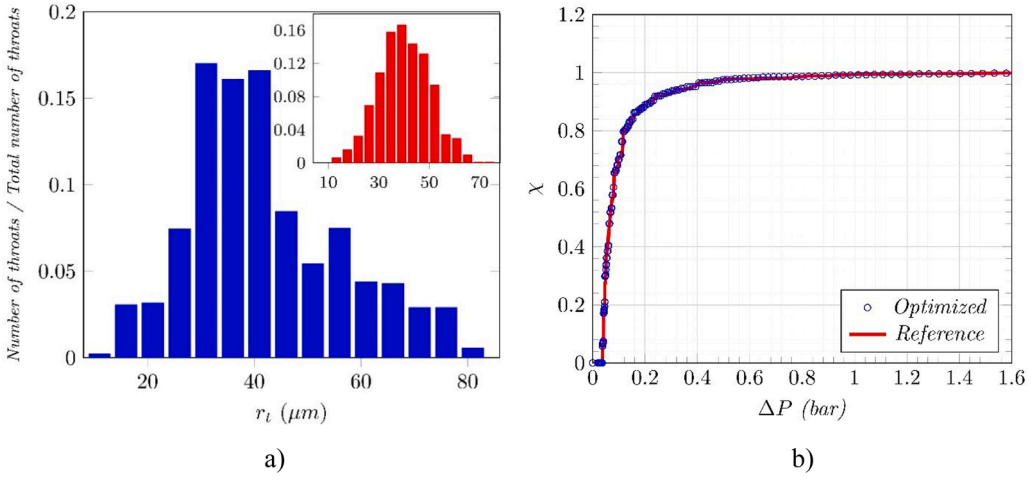

Fig. 6. Results of the optimization procedure for a case where the reference p.d.f. is Gaussian. (a) TSD of the optimized network (the inset shows the reference TSD). (b) FFDP curve for the reference network and the optimized network.

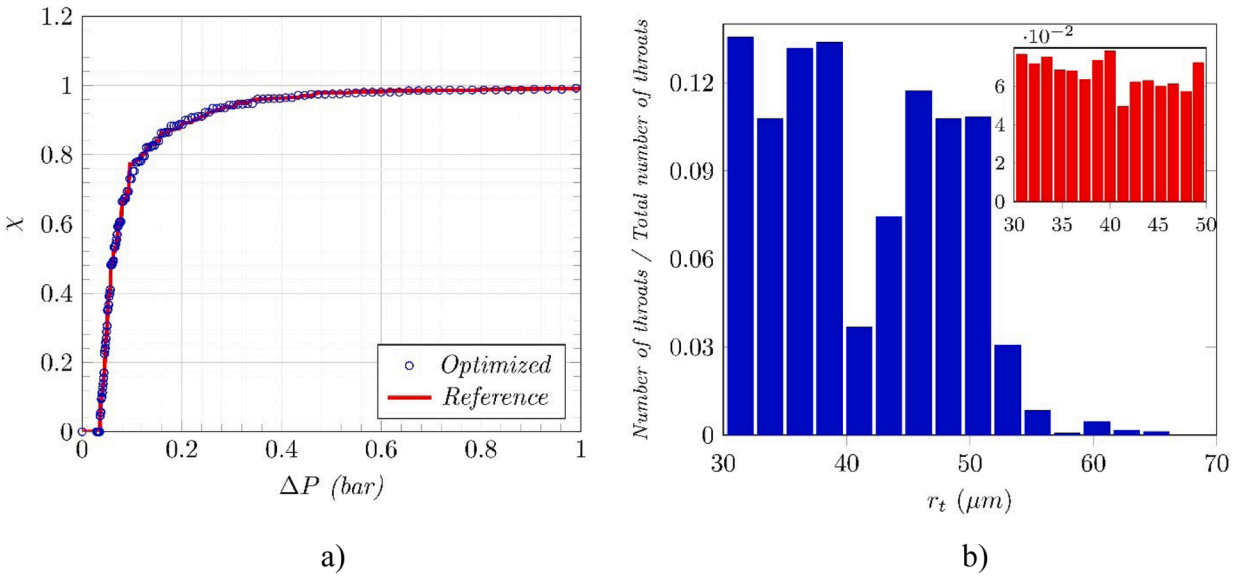

Fig. 7. Results of optimization procedure for a case where the reference p.d.f. is uniform. (a) FFDP curve for the reference network and the optimized network. (b) TSD of the optimized network (the inset shows the reference TSD).

were measured and are available. For the present study, this means that the curve $P_c(S)$ can be computed for the reference network as well as for all the networks generated during the optimization procedure. The algorithm for computing the retention curve in a network is described in Maalal et al. (2021) and therefore is not further again reported here. The optimization procedure is completely analogous to the one described in this reference when both the retention curve and the relative permeability curve is used. The sole modification is the use of χ (Eq. (12)) in place of Q_n in Maalal et al. (2021).

7.2. Results

In Fig. 8, the results on the retention curve, the FFDP curve and the TSD resulting from the optimization procedure are reported together with the corresponding quantities for the reference network.

As can be seen from the comparison between Figs. 6 and 8, using both the retention and FFDP curves in the optimization process leads to significantly better results. This is also confirmed by the results reported in Table 4. It can be noted in Fig. 8a and b that the retention and FFDP curves resulting from the optimization procedure reproduce very well the corresponding curves of the reference case. As shown earlier (Maalal et al., 2021), it is of course possible to develop the inverse optimization procedure using only the retention curve. For completeness, the results obtained with this strategy are also indicated in Table 4. As can be seen, results when only the retention curve is used are slightly better than when only the FFDP curve is employed. However, the best results are obtained when both the retention and the FFDP curves are used.

In Fig. 9 and Table 5, results obtained for the case of the uniform distribution depicted in the inset of Fig. 9c are reported. A comparison of Fig. 9 with Fig. 7 shows that here, again, significantly better results are obtained when the FFDP curve is used in conjunction with the retention curve in the optimization process. However, results for the uniform distribution can be judged as slightly less satisfactory than for the Gaussian distribution. In particular, it can be noticed that the procedure leads to identify a few throat sizes greater than the greatest throat size in the reference distribution. Again, this can be attributed to the procedure used to estimate the maximum radius of the distribution with the factor 1.3, as mentioned at the end of Section 6.2.

Nevertheless, to further illustrate the capabilities of the inverse optimization procedure as above described, two additional tests were performed considering a reference Log-normal distribution (as depicted in Fig. 10a) and the expected more challenging bimodal distribution depicted in Fig. 11a. For these cases, only the full optimization procedure, i.e., the one combining both the $P_c(S)$ and $\chi(\Delta P)$ curves was used. As can be seen from Figs. 10 and 11, respectively corresponding to the Log-normal and bimodal distributions, and from Table 6, results are quite satisfactory. Here also, the match between the reference capillary pressure and FFDP curves and the curves resulting from the optimization procedure is excellent although they are not reported here for the sake of brevity. Finally, from the four reference TSD tested in this study, the less satisfactory results were obtained for the uniform TSD, mainly because of the uncertainty associated with the specification of the upper bound radius of the distribution.

8. Discussion

The TSD identification based on the optimization procedure clearly leads to much better results than the conventional FFDP approach. However, several simplifications were introduced. The displacement was computed neglecting the viscous pressure drop in the displaced fluid during the transient period occurring right after the inlet pressure increase until a new steady–state (equilibrium) is reached. As explained before, this approximation was made because the FFDP procedure is based on small inlet pressure increments, corresponding to a few meniscus displacements between two successive pressure steps. Nevertheless, it would be interesting to test the quality of the approximation from comparisons with more advanced models, such as dynamic pore networks for instance, (see e.g., Joekar-Niasar et al., 2010; Joekar-Niasar and Hassanizadeh, 2012). Trapping was neglected because it is exacerbated in 2D networks compared to 3D networks. In this respect, it would be interesting to consider 3D networks with trapping. It may be expected that some pore sizes are unidentified because of trapping since the trapped regions cannot be visited by the menisci probing the pore space.

Also a network of identical structure, i.e., a square network, was considered for the reference network and the networks generated in the optimization procedure. Obviously, this is a serious limitation. However, the idea was to first test the procedure for this particular case where the network structure is known. The next step would be to test the procedure considering a reference network structure different from the one used in the optimization procedure and explore whether it is still possible to reasonably identify the TSD. In this respect, the connectivity,

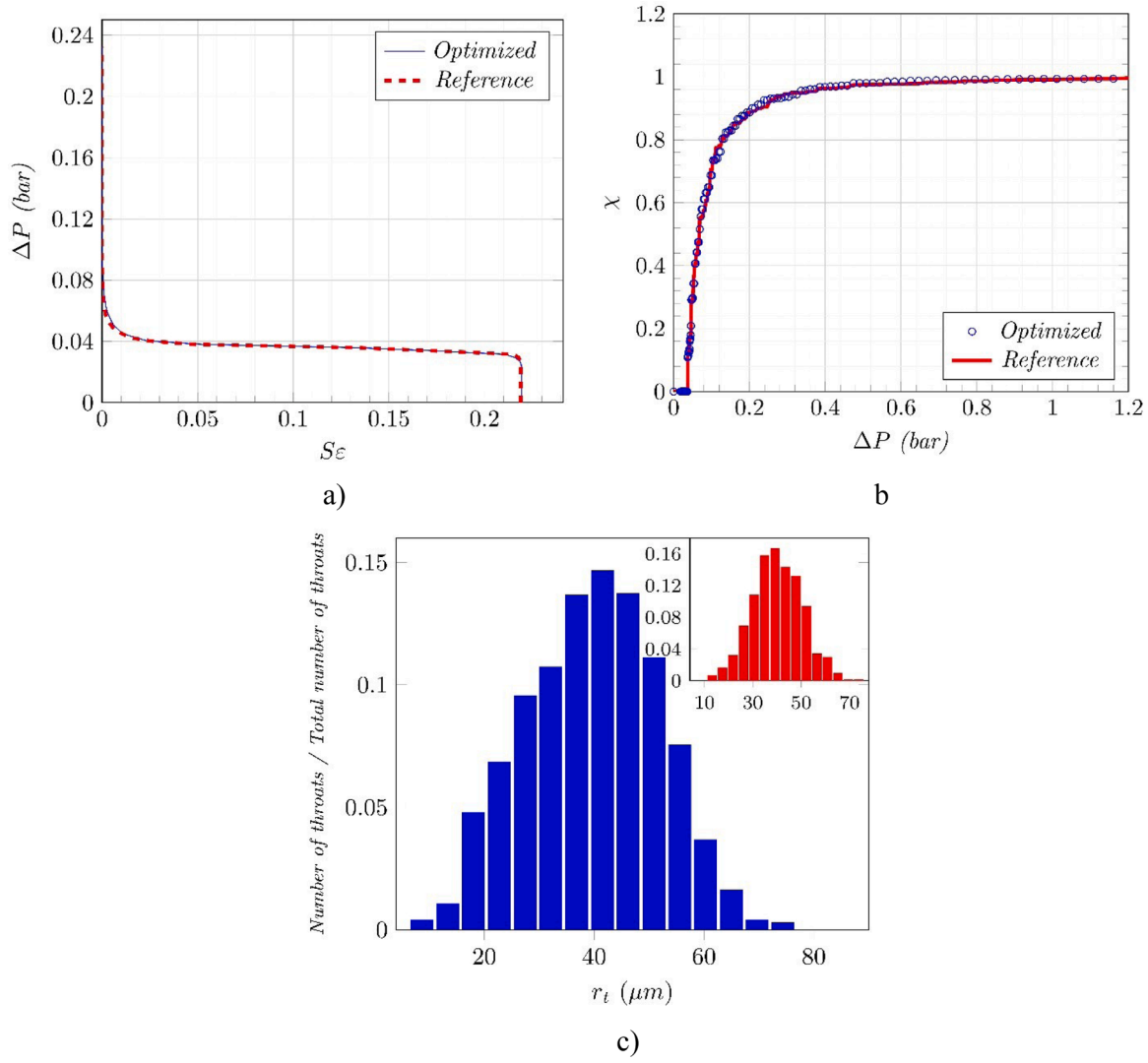

Fig. 8. Results of the optimization procedure when both the FFDP and the retention curves are used for a case where the reference p.d.f. is Gaussian (the mean radius and standard deviation are respectively equal to 40 μm and 10 μm). (a) retention curve and (b) FFDP curve for the reference network and the optimized network. Note that $\Delta P = P_i - P_o$ corresponds to P_c. (c) TSD of the optimized network (the inset shows the reference TSD).

Table 4
Comparison between the reference TSD and the TSD obtained from the optimization procedure. Case where the reference TSD is the Gaussian TSD depicted in the inset of Fig. 8c.

		P_c only		*FFDP* only		both *FDDP* and P_c	
Statistical Moments (μm)	Real TSD	Obtained TSD	Relative Error (%)	Obtained TSD	Relative Error (%)	Obtained TSD	Relative Error (%)
Mean	42.05	41.11	2.3	43.65	3.8	41.96	0.21
Standard deviation	10.2	10.3	0.9	13.16	33.33	10.14	0.59
Skewness	-0.22	-0.42	-	0.41	-	-0.36	-
Kurtosis	2.71	2.93	7.66	2.95	8.86	2.86	5.54

i.e., the number of adjacent pores connected to a given pore, appears as an important parameter (Meyers et al., 2001; Mourhatch et al., 2011). This suggests to include the connectivity as a parameter to be identified in the optimization procedure. Some of the above elements were also discussed in Maalal et al. (2021) where complementary aspects can be found. In this reference, it was concluded that the combined use of the retention and displacing fluid relative permeability curves leads to better results than the use of the relative permeability curve alone. A similar conclusion is reached here since the combined use of the retention and FFDP curves leads to the best results for all the distributions tested.

The combined use of the retention curve and FFDP curves is thus recommended. For the TSD identification of thin porous media with throats in the micronic range, such as the diffusion medium used in fuel cells for example (Fairweather et al., 2010; Gostick et al., 2008; Park et al., 2012), obtaining both curves should not be a problem. For thin nanoporous media, the combined approach could be more difficult to use because measurement of the retention curve can be a challenging

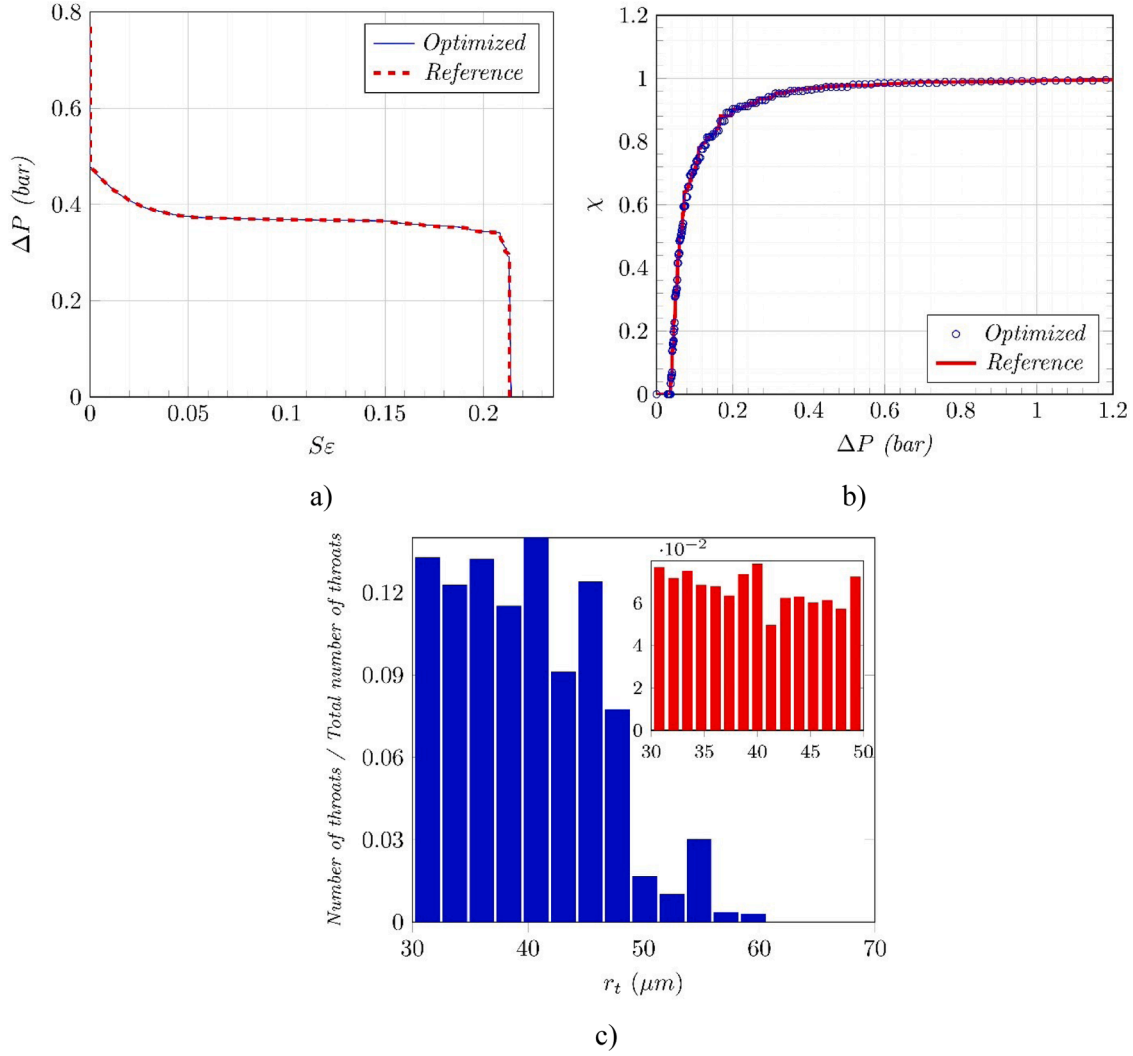

Fig. 9. Results of the optimization procedure when both the FFDD and retention curves are used for a case where the reference p.d.f. is uniform (the maximum and minimum radius are respectively 50 μm and 30 μm). (a) retention curve and (b) FFDP curve for the reference network and the optimized network. Note that $\Delta P = P_i - P_o$ corresponds to P_c. (c) TSD of the optimized network (the inset shows the reference TSD).

Table 5
Comparison between the reference TSD and the TSD obtained from the optimization procedure. Case where the reference TSD is the uniform TSD depicted in the inset in Fig. 9c.

		P_c only		*FFDP* only		both *FFDP* and P_c	
Statistical Moments (μm)	Real TSD	Obtained TSD	Relative Error (%)	Obtained TSD	Relative Error (%)	Obtained TSD	Relative Error (%)
Mean	41.16	41.25	0.21	42.8	3.98	40.96	0.49
Standard deviation	6.08	6.14	1.01	7.19	18.25	5.85	3.78
Skewness	-0.6	-0.04	-	-0.34	-	-0.49	-
Kurtosis	1.81	2.9	60.17	1.71	5.44	2.6	43.65

task. In practice, the retention curve measurement implies to place a porous membrane at the outlet of the porous medium of interest. The pores in the outlet membrane must be smaller than the pores in the porous medium to be characterized in order to prevent the non-wetting fluid to exit the sample. Using a membrane with the required pore size when the pores in the porous medium of interest are in the nanometer range may be a difficulty in practice. This problem is not encountered with the FFDP technique. Also, the FFDP technique can be performed using a pair of immiscible liquids with a relatively low interfacial tension so as to generate the displacement with reasonably low-pressure differences even in the presence of nano-pores. Thus, in that case, the FFDP technique combined with the optimization procedure is an interesting option to characterize the TSD.

9. Conclusion

Pore network simulations were developed in order to evaluate the fluid-fluid displacement porosimetry (FFDP) technique. It was suggested that two types of microstructure elements, namely pore bodies and pore throats, must be distinguished in the pore space. It was argued that the

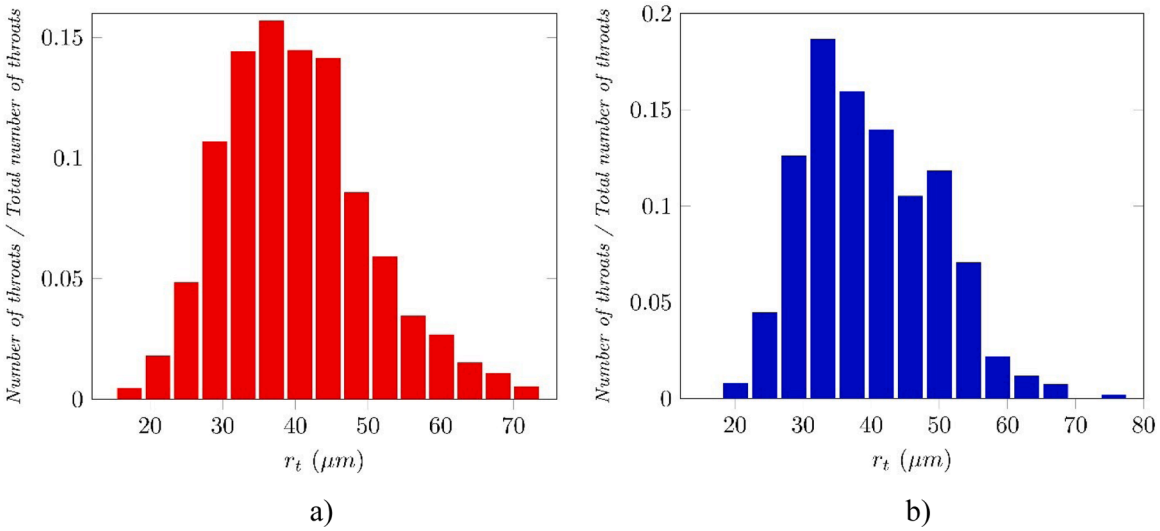

Fig. 10. Reference Log-normal TSD (a)) and TSD obtained from the optimization procedure using both the FFDP and capillary pressure curves as target data (b)). 30 × 30 square network.

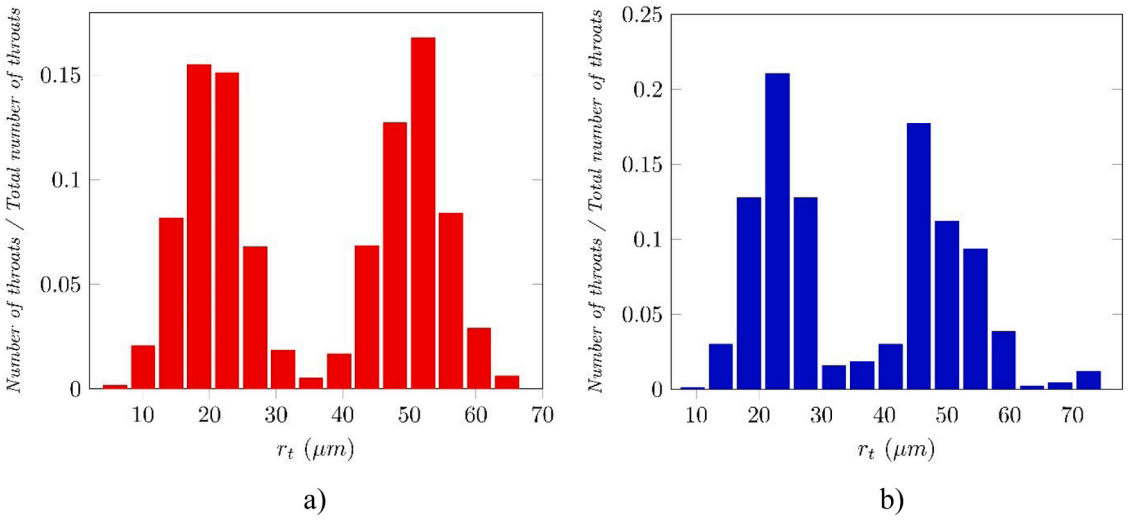

Fig. 11. Reference bimodal TSD (a)) and TSD obtained from the optimization procedure using both the FFDP and capillary pressure curves as target data (b)). 30 × 30 square network.

Table 6
Comparison between the reference TSD and the TSD obtained from the optimization procedure making use of both the capillary pressure and FFDP curves as target data. Cases where the reference TSD is the Log-normal TSD depicted in Fig. 10a and the bimodal TSD depicted in Fig. 11a.

	Log-normal TSD			Bimodal TSD		
Statistical Moments (μm)	Real TSD	Obtained TSD	Relative Error (%)	Real TSD	Obtained TSD	Relative Error (%)
Mean	40.84	41.38	1.31	36.16	36.23	0.19
Standard deviation	9.33	10.01	7.25	16.06	14.63	8.92
Skewness	0.05	0.08	-	-0.22	0.11	-
Kurtosis	2.62	2.73	4.13	1.37	1.69	23.33

distribution commonly obtained with the FFDP technique was the throat size distribution (TSD) rather than the pore body size distribution (PBSD) in accordance with the physical process at play (drainage). Direct Pore network simulations indicate that the commonly used FFDP procedure for identifying the TSD from the FFDP curve introduces a bias toward unrealistic small sizes as a consequence of the viscous pressure drop in the displacing fluid. The thicker the porous medium, the greater is the bias. In practice, this means that the results obtained with the commonly used FFDP procedure should not be regarded as representative of the real TSD when the pore space structure is significantly different from a system of straight non-interconnected quasi-cylindrical pores.

A significantly more sophisticated procedure, combining pore network simulations of the immiscible displacement and an optimization technique based on a hybrid genetic and hill climbing algorithm recently reported in the literature was then tested to improve the TSD identification from the FFDP raw data. This procedure leads to much better results than the usual FFDP interpretation and allows eliminating the bias toward unrealistic small throats. Furthermore, it was shown that the TSD identification could be still improved by considering the retention curve in addition to the FFDP curve in the optimization procedure.

The efficiency of the method proposed here is to the cost of a significantly less simple procedure than the commonly used FFDP interpretation technique. The latter is analytical whereas the

optimization procedure implies repeated numerical simulations of the immiscible displacements in the pore space. In addition, several simplifications were introduced to test the improved optimization procedure. In particular, identical network structure and size were considered in the reference network and the various networks generated during the optimization procedure. The variability in the pore size was neglected, considering only the throat size distribution. Owing to these simplifications, solving the problem consisting in identifying the TSD (and the PBSD) from macroscopic data such as the FFDP and capillary pressure curves clearly requires further work.

CRediT authorship contribution statement

Otman Maalal: Methodology, Writing – original draft, Writing – review & editing. **Marc Prat:** Conceptualization, Software, Writing – original draft, Writing – review & editing. **René Peinador:** Writing – review & editing. **Didier Lasseux:** Conceptualization, Writing – original draft, Writing – review & editing.

Declaration of Competing Interest

The authors declare that they have no known competing financial interests or personal relationships that could have appeared to influence the work reported in this paper.

Acknowledgments

This research was supported by the Project “PEMFC – SUDOE” – SOE1/P1/E0293 which is co-financed by the European Regional Development Fund in the framework of the Interreg Sudoe programme.

References

Agaesse, T., Lamibrac, A., Buechi, F., Pauchet, J., Prat, M., 2016. Validation of pore network simulations of *ex-situ* water distributions in a gas diffusion layer of proton exchange membrane fuel cells with X-ray tomographic images. J. Power Sources 331, 462–474.

Blunt, M.J., 2001. Flow in porous media-pore-network models and multiphase flow. Curr. Opin. Colloid Interface Sci. 6, 197–207.

Blunt, M.J., Jackson, M.D., Piri, M., Valvatne, P.H., 2002. Detailed physics, predictive capabilities and macroscopic consequences for pore-network models of multiphase flow. Adv. Water Res. 25 (8–12), 1069–1089.

Bondino, I., Hamon, G., Kallel, W., Kachuma, D., 2013. Relative permeabilities from simulation in 3D rock models and equivalent pore networks: critical review and way forward. Petrophysics 54 (6), 538–546.

Calvo, J.I, Peinador, R.I., Prádanos, P., Bottino, A., Comite, A., Firpo, R., Hernández, A., 2015. Porosimetric characterization of polysulfone ultrafiltration membranes by image analysis and liquid–liquid displacement technique. Desalination 357, 84–92.

Dullien, F.A.L., 1991. Porous Media: Fluid Transport and Pore Structure. Academic Press.

Fairweather, J.D., Cheung, P., Schwartz, D.T., 2010. The effects of wetproofing on the capillary properties of proton exchange membrane fuel cell gas diffusion layers. J. Power Sources 195, 787–793.

Gostick, J.T., Ioannidis, M.A., Fowler, M.W., Pritzker, M.D., 2008. Direct measurement of the capillary pressure characteristics of water–air–gas diffusion layer systems for PEM fuel cell. Electrochem. Commun. 10, 1520–1523.

Islam, M.A., Hossain, M.S., Garcia-Payo, C., Khayet, M., Ulbricht, M., 2020. Mixed Poiseuille-Knudsen flow model for gas liquid displacement porometry data treatment. J. Membr. Sci. 612, 118422.

Joekar-Niasar, V., Hassanizadeh, S.M., Leijnse, A., 2008. Insights into the relationships among capillary pressure, saturation, interfacial area and relative permeability using pore-network modelling. Transp. Porous Media 74, 201–219.

Joekar-Niasar, V., Hassanizadeh, S.M., Dahle, H.K., 2010. Non-equilibrium effects in capillarity and interfacial area in two-phase flow: dynamic pore-network modelling. J. Fluid Mech. 655 (1), 38–71.

Joekar-Niasar, V., Hassanizadeh, S.M., 2012. Analysis of fundamentals of two-phase flow in porous media using dynamic pore-network models: a review. Crit. Rev. Environ. Sci. Technol. 42 (18), 1895–1976.

Lenormand, R., Touboul, E., Zarcone, C., 1988. Numerical models and experiments on immiscible displacements in porous media. J. Fluid Mech. 189, 165–187.

Meyers, J.J., Nahar, S., Ludlow, D.K., Liapis, A.I., 2001. Determination of the pore connectivity and pore size distribution and pore spatial distribution of porous chromatographic particles from nitrogen sorption measurements and pore network modelling theory. J. Chromatogr. A 907 (1-2), 57–71.

Maalal, O., Prat, M., Peinador, R., Lasseux, D., 2021. Determination of the throat size distribution of a porous medium as an inverse optimization problem combining pore network modeling and genetic and hill climbing algorithms. Phys. Rev. E 103, 023303.

Morison, K.R., 2008. A comparison of liquid-liquid porosimetry equations for evaluation of pore size distribution. J. Membr. Sci. 325, 301–310.

Mourhatch, R., Tsotsis, T.T., Sahimi, M., 2011. Determination of the true pore size distribution by flow permporometry experiments: an invasion percolation model. J. Membr. Sci. 367, 55–62.

Park, S., Lee, JW., Popov, B.N., 2012. A review of gas diffusion layer in PEM fuel cells: materials and designs. Int. J. Hydrog. Energy 37, 5850–5865.

Peinador, R.I., Calvo, J.I., Ben Aim, R., 2020. Comparison of capillary flow porometry (CFP) and liquid extrusion porometry (LEP) techniques for the characterization of porous and face mask membranes. Appl. Sci. 10, 5703.

Peinador, R.I., Calvo, J.I., Prádanos, P., Palacio, L., Hernández, A., 2010. Characterization of polymeric UF membranes by liquid-liquid displacement porosimetry. J. Membr. Sci. 348, 238–244.

Raeini, A.Q., Bijeljic, B., Blunt, M.J, 2017. Generalized network modeling: network extraction as a coarse-scale discretization of the void space of porous media. Phys. Rev. E 96, 013312.

Tanis-Kanbur, M.B., Peinador, R.I., Hu, X., Calvo, J.I., Chew, J.W., 2019. Membrane characterization via evapoporometry (EP) and liquid-liquid displacement porosimetry (LLDP) techniques. J. Membr. Sci. 586, 248–258.

Wilkinson, D., Willemsen, J.F., 1983. Invasion percolation: a new form of percolation theory. J. Phys. A Math. Gen. 16, 3365–3376.

Xiong, Q., Baychev, T.G., Jivkov, A.P., 2016. Review of pore network modelling of porous media: experimental characterizations, network constructions and applications to reactive transport. J. Contam. Hydrol. 192, 101–117.

Xu, B., Yortsos, Y.C., Salin, D., 1998. Invasion percolation with viscous forces. Phys. Rev. E 57, 739.

Zhou, D., Blunt, M., Orr, F.M., 1997. Hydrocarbon drainage along corners of noncircular capillaries. J. Colloid Interface Sci. 187, 11–21.